Vietnam Journal of Catalysis and Adsorption
Tạp chí xúc tác và hấp phụ Việt Nam

https://jca.edu.vn

# Synthesis of $Cu_2O$-$BiVO_4$ catalysts used as high-performance photoanodes for photoelectrochemical water splitting

Nguyen Nguyen Hai[1], Cao Thi Anh Kien[1], Nguyen Vu Hoang Phuong[2], Tran Thi Khanh Linh[1], Nguyen Thi Mo[1,*]

[1] *Hanoi National University of Education, 136 Xuan Thuy, Cau Giay, Hanoi, VIETNAM*
**Email: ntmo@hnue.edu.vn*

ARTICLE INFO

Received: 14/12/2024
Accepted: 27/02/2025
Published: 30/03/2025

*Keywords:*
Photoelectrochemical water splitting, copper(I) oxide, bismuth vanadate, photoanode.

ABSTRACT

Herein, $Cu_2O$ and $BiVO_4$ were synthesized using different methods. The structure, morphology, light absorption ability of synthesized materials were examined by XRD, SEM, DRS UV-Vis, PL and photoelectrochemical performance. was determined by LSV and EIS methods. $BiVO_4$ synthesized by the electrodeposition exhibits lower crystallinity and smaller particle sizes, leading to higher photocurrent density (0.55 $mA{\cdot}cm^{-2}$ at 1.23 V versus RHE). The combination of $Cu_2O$ and $BiVO_4$ improves charge transfer ability and photocatalytic performance, with a current density of 1.23 $mA{\cdot}cm^{-2}$ at 1.23 V vs RHE, demonstrating the material's potential as a photoanode in photoelectrochemical water splitting.

## Introduction

In recent years, global energy demand has surged due to industrialization and population growth. The depletion and environmental harm of fossil fuels raises concerns about energy sustainability and pollution. Producing clean, renewable energy is critical, and hydrogen stands out as a promising solution due to its high energy density, emission-free nature, and long-term storage ability [1, 2]. However, current hydrogen production, primarily via steam methane reforming, generates significant greenhouse gases. Efforts are focused on developing green technologies for water splitting, including photoelectrochemical (PEC) methods, first introduced in 1972 by Fujishima and Honda using $TiO_2$ under UV light. PEC water splitting uses solar energy to generate hydrogen and oxygen, with efficiency limited by the slow kinetics of the oxygen evolution reaction (OER). The efficiency of OER largely relies on employed catalytic materials, highlighting the need to enhance photocatalyst performance. Therefore, the development of high-performance photoanode materials is essential for improving PEC efficiency [3, 4]. Among potential photoanode materials, $BiVO_4$ has garnered attention for its ability to absorb visible light (bandgap ~2.4 eV), long-term stability, and appropriate band edges alignment with oxygen evolution and hydrogen evolution potentials. $BiVO_4$ is also composed of non-toxic, abundant elements and remains stable in near-neutral solutions, making it suitable for PEC applications. Nonetheless, inherent limitations like inefficient transfer of photogenerated charges, and rapid recombination of electron-hole pairs hinder the photocatalytic performance of $BiVO_4$. To address these challenges, various approaches have been proposed, including formation of heterojunctions [5, 6], doping with metals or non-metals [7, 8], and surface modifications [9, 10]. Among these methods, heterojunction construction stands out as a particularly effective strategy. Majumder *et. al.* demonstrated that a $BiVO_4/Fe_2TiO_5/Co_3O_4$ heterojunction achieved a 5.3-fold increase in photocurrent density along with a significant cathodic shift compared to bare $BiVO_4$ photoanodes [11]. Liu et al. observed that a $Fe_3CoPPc$-$BiVO_4$ hybrid produced an exceptional oxygen evolution rate of 4557 μmol $g^{-1}$ $h^{-1}$ in the presence of iodate under visible light, nearly two orders of magnitude

https://doi.org/10.62239/jca.2025.007

higher than pristine $BiVO_4$ [12]. Among well-studied semiconductors, $Cu_2O$ is characterized by its narrow direct band gap (2.1–2.3 eV), high absorption coefficient, non-toxic nature and excellent carrier mobility [13, 14]. Heterojunction between $Cu_2O$, a p-type semiconductor, and $BiVO_4$, an n-type semiconductor, can enhance charge separation and reduce recombination of photogenerated electron-hole pairs, improving PEC performance. This synergy also broadens light absorption range and increases the efficiency of solar energy utilization. This study focuses on the effect of heterojunction of $Cu_2O$-$BiVO_4$ photoanode on its activity for photoelectrochemical water splitting.

## Experimental

### *Chemicals*

All chemicals, including bismuth nitrate pentahydrate ($Bi(NO_3)_3{\cdot}5H_2O$), vanadyl acetylacetonate ($C_{10}H_{14}O_5V$), ammonium metavanadate ($NH_4VO_3$), dimethyl sulfoxide ($C_2H_6OS$), ethylenediaminetetraacetic acid (EDTA), ethylene glycol (EG), nitric acid ($HNO_3$), copper sulfate pentahydrate ($CuSO_4{\cdot}5H_2O$); sodium tartrate dihydrate ($Na_2C_4H_4O_6{\cdot}2H_2O$); glucose; urea and sodium hydroxide were of analytical grade and procured from China. All these chemicals were utilized without further purification. Fluorine-doped tin oxide (FTO) substrates were cut into 1.0 cm × 2.5 cm pieces. They were cleaned using soap and subsequently sonicated in acetone, ethanol, and deionized water for 30 minutes each.

### *Synthesis of $BiVO_4$ by chemical precipitation*

For the chemical precipitation method, 8.730 g of $Bi(NO_3)_3{\cdot}5H_2O$ was dissolved in 250 mL of 1M $HNO_3$. Then, 2.106 g of $NH_4VO_3$ was added to the solution, and the mixture was stirred for 1 hour at 40°C. After adding 9,00 g of urea, the solution was kept in 80°C oil bath for 24 hours. After centrifuging, washing, and drying, the powder was collected and denoted as $BiVO_4$-CP. The powder was loaded on FTO by doctor blade method, dried at 60°C for 6 hours, and calcined at 450°C for 2 hours. The final sample is denoted as $BiVO_4$-CP/FTO.

### *Synthesis of $Cu_2O$ by chemical reduction*

8.725 g of $CuSO_4{\cdot}5H_2O$ was dissolved in 50 mL of distilled water. Then, 2.80 g of NaOH and 6.02 g of $Na_2C_4H_4O_6$ were dissolved in 50 mL of distilled water. Sodium tartrate solution was mixed with copper sulfate solution to form copper tartrate alkaline solution with continuous stirring at 60 °C. Then 50 mL of 1.4 M glucose was added to copper tartrate alkaline solution, forming a red-brick $Cu_2O$ precipitate. The pH of the solution was adjusted to 10. The obtained $Cu_2O$ precipitate was filtered, washed, and dried with acetone. This sample was designated as $Cu_2O$. $Cu_2O$ was deposited on FTO glass using the doctor blade method, dried at 60°C for 6 hours, and calcined at 450°C for 2 hours and designated as $Cu_2O$/FTO.

### *Synthesis of $BiVO_4$ thin film by electrodeposition*

Bi metal was deposited on FTO glass through electrochemical deposition in a solution containing 0.4852 g $Bi(NO_3)_3{\cdot}5H_2O$ in 100 mL EG and 50 mL water. A three-electrode setup was employed, comprising an FTO working electrode, an Ag/AgCl reference electrode, and a platinum counter electrode, with deposition performed at -0.6 V (vs. Ag/AgCl) for 500 seconds. The Bi-coated electrode was washed, dried, and coated with 200 µL of 0.2M $C_{10}H_{14}O_5V$ solution in $C_2H_6OS$. After calcination at 450°C for 2 hours, the electrode was immersed in 1M NaOH for 30 minutes to remove residual $V_2O_5$, washed, dried at 60°C, and denoted as $BiVO_4$-ED/FTO.

### *Synthesis of $Cu_2O$-$BiVO_4$ thin film by electrodeposition*

$Cu_2O$ was electrodeposited on $BiVO_4$-ED/FTO synthesized by above procedure with $BiVO_4$-ED/FTO working electrode, which was immersed in an electrolyte solution containing 0.02 M $Cu(CH_3COO)_2$ and 0.08 M $CH_3COOH$. Electrolysis was performed at -0.3 V vs Ag/AgCl for 200 seconds. At this condition, the following reaction occurs: $2Cu^{2+}+H_2O+2e^- \rightarrow Cu_2O+2H^+$. The prepared photoanode was thoroughly rinsed and dried at 60°C. The resulting product is designated as the $Cu_2O$-$BiVO_4$-ED/FTO

### *Material Characterization*

The structure of synthesized samples was determined by powder X-ray diffraction (XRD) using D8 Advance-Bruker diffractometer with Cu-Kα radiation (λ=1.5406 Å) in 2θ range of 20–80°. Scanning electron microscopy (SEM) was examined with a JEOL JSM-5410LV microscope. UV-vis diffuse reflectance spectroscopy (DRS) evaluated optical properties using $BaSO_4$ as a reference in a Shimadzu UV-2600. Photoluminescence (PL) spectra were recorded with a Hitachi F-4600 spectrophotometer at a 210 nm and 520 nm excitation wavelength.

### *Study the Photoelectrochemical Performance*

Photoelectrochemical measurements were carried out in a three-electrode system by linear sweep voltammetry (LSV) method with electrodes immersed in 0.1M phosphate buffer solution (PBS, pH 7.4). A 200W lamp was illuminated to a 1 $cm^2$ photoanode. Current-voltage curves were recorded at 20 mV/s scan rate, with potential reference converted from Ag/AgCl to the reversible hydrogen electrode (RHE) using the following equation:

https://doi.org/10.62239/jca.2025.007

$$E_{RHE}=E_{Ag/AgCl}+E_{Ag/AgCl\ vs.\ NHE}+0.059\cdot pH$$

where $E_{Ag/AgCl\ vs.\ NHE}$=0.1976 V at 20°C

Electrochemical impedance spectroscopy (EIS) measurements spanned frequencies from 10 kHz to 100 MHz with a 5 mV AC voltage.

## Results and discussion

### *XRD results*

The crystalline structure of the synthesized samples was analyzed using XRD. The XRD profiles for $Cu_2O$, $BiVO_4$-CP, $BiVO_4$-ED/FTO, $Cu_2O$-$BiVO_4$-ED/FTO are shown in the Fig. 1.

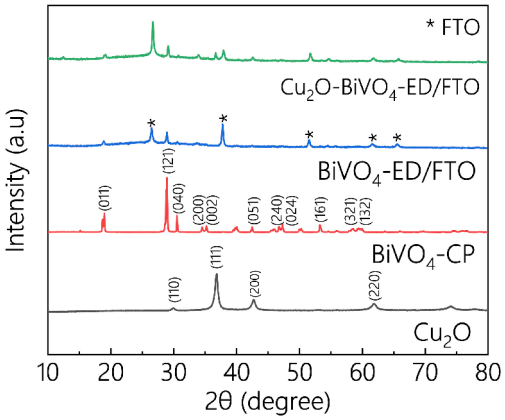


Fig. 1: XRD patterns of $Cu_2O$, $BiVO_4$-CP, $BiVO_4$-ED/FTO, $Cu_2O$-$BiVO_4$-ED/FTO

XRD pattern of $Cu_2O$ displays diffraction peaks at 2θ = 29.55°, 36.41°, 42.29°, and 61.34°characteristic for cubic $Cu_2O$ single-phase These peaks are indexed to the (110), (111), (200), and (220) facets (JCPDS: 65-3288). For $BiVO_4$-CP, the characteristic diffraction peaks observed at 2θ angles of 18.9°, 28.9°, 30.6°, 34.5°, 35.2°, 39.5°, 40.2°, 42.5°, 46.8°, 47.3°, 50.3°, 53.3°, 58.5°, and 59.5°. corresponding to the crystal planes (011); (121), (040), (200), (002), (211), (112), (051), (240), (042), (202), (161), (321), and (132) of monoclinic $BiVO_4$ (JCPDS 14-0688). No diffraction peaks of $Bi_2O_3$ or tetragonal $BiVO_4$ were detected, confirming the formation of a pure monoclinic $BiVO_4$ phase.
For $BiVO_4$-ED/FTO and $Cu_2O$-$BiVO_4$-ED/FTO, diffraction peaks of the FTO at 26.7°, 37.9°, 51.8°, 61.9°, and 65.7° are observed. Besides, the characteristic peaks for monoclinic $BiVO_4$ facets (121), (040), and (200) still appear but become broader and less intense, signifying reduced crystallinity. Additionally, peaks of cubic $Cu_2O$ at 36.41°, 42.29°, and 61.34° can be also observed in XRD pattern of $Cu_2O$-$BiVO_4$-ED/FTO with significantly lower intensity. The XRD results indicate the successful deposition of $BiVO_4$ and $Cu_2O$ on the surface of FTO.

### *SEM results*

To examine the morphology of synthesized samples, SEM analysis was conducted, and the resulting images are presented in Fig. 2. $Cu_2O$ consists of relatively uniform spherical particles with sizes of about 1 µm. $BiVO_4$-CP consists of irregularly aggregated particles with a rhombic dodecahedral shape and varying sizes from several hundred nanometers to a few microns. These particles cluster together to form larger aggregates. Meanwhile, $BiVO_4$-ED is composed of nanoparticles with grain sizes smaller than 200 nm. $Cu_2O$-$BiVO_4$-ED forms very small, uniform particles with sizes below 100 nm on the FTO surface. The particle size of samples synthesized by electrodeposition methods reduces significantly, forming nanocrystals and creating an even surface on FTO as compared to those prepared by chemical precipitation. This is probably due to the decrease in the crystallinity of the electrodeposited samples. These results align well with analysis of the materials by the XRD method.

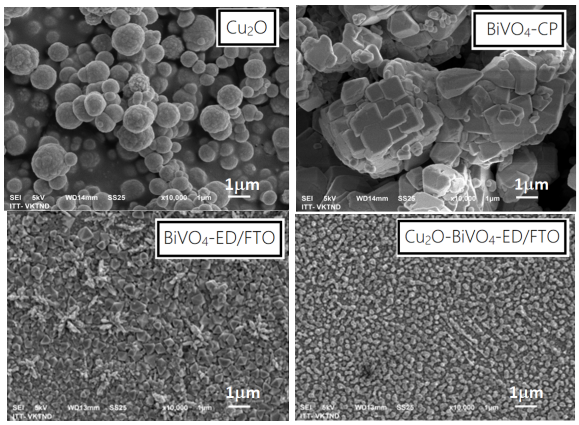


Fig. 2: SEM images of $Cu_2O$, $BiVO_4$-CP, $BiVO_4$-ED/FTO, $Cu_2O$-$BiVO_4$-ED/FTO

### *UV-Vis DRS results*

The DRS UV-Vis results in Fig. 3a for all prepared samples indicate that all synthesized catalysts are photoactive. The UV-Vis spectra of the synthesized materials show absorption peaks in the visible light region with relatively high absorbance intensity. The absorption peaks for $Cu_2O$, $BiVO_4$-CP, $BiVO_4$-ED/FTO, $Cu_2O$-$BiVO_4$-ED/FTO were observed at wavelengths of 490 nm, 472 nm, 437 nm, and 454 nm, respectively.
The bandgap values determined using the Kubelka–Munk method and Tauc plots are presented in fig. 3b. The bandgap energies for the $Cu_2O$, $BiVO_4$-CP, $BiVO_4$-ED/FTO, $Cu_2O$-$BiVO_4$-ED/FTO samples are 1.92 eV, 2.38 eV, 2.45 eV, and 1.82 eV, respectively. Additionally, it is evident that when $Cu_2O$ is combined with $BiVO_4$ on the FTO substrate, the bandgap energy decreases. This

https://doi.org/10.62239/jca.2025.007

suggests an interaction between $Cu_2O$ and $BiVO_4$, resulting in a material with improved light absorption capabilities, particularly in the longer wavelength region.

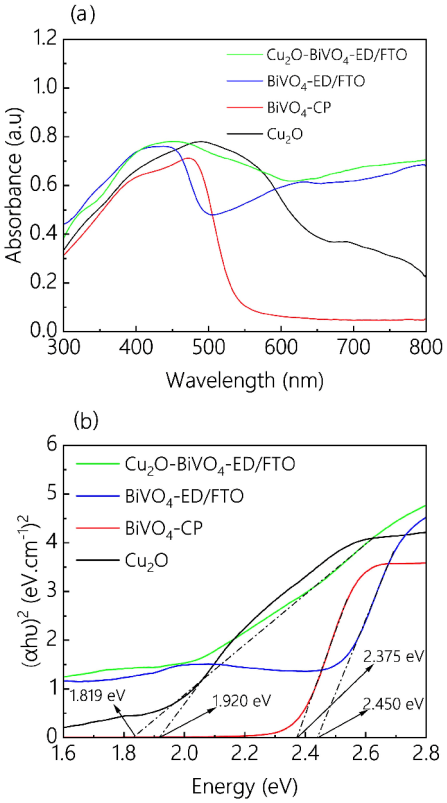


Fig. 3: DRS UV-Vis spectra (a) and Tauc plots (b) of $Cu_2O$, $BiVO_4$-CP, $BiVO_4$-ED/FTO, $Cu_2O$-$BiVO_4$-ED/FTO

### *PL results*

The fluorescence spectra of $BiVO_4$-CP, $BiVO_4$-ED/FTO, $Cu_2O$-$BiVO_4$-ED/FTO at 210 nm excitation wavelength are shown in Fig. 4a. It emits fluorescence at approximately 421 nm. This emission peak is characteristic of the fluorescence ability of $BiVO_4$. When $BiVO_4$ is electrodeposited on FTO surface, the fluorescence intensity at 421 nm decreases. This result may indicate that the recombination of electron-hole pairs in $BiVO_4$-ED is lower than that in $BiVO_4$-CP. Notably, when $Cu_2O$ is combined with $BiVO_4$, fluorescence emission intensity at 421 nm decreases significantly. This is likely due to the interaction between $Cu_2O$ and $BiVO_4$, facilitating electron-hole separation. Similarly, when $Cu_2O$-containing materials are excited at 520 nm, a fluorescence emission peak is observed at around 780 nm, which is characteristic of $Cu_2O$ fluorescence. It is evident that the incorporation of $Cu_2O$ with $BiVO_4$ also significantly reduces the fluorescence intensity, suggesting lower recombination of photogenerated electron-hole pairs in the $Cu_2O$ component and, therefore, creating materials with better expected photocatalytic performance.

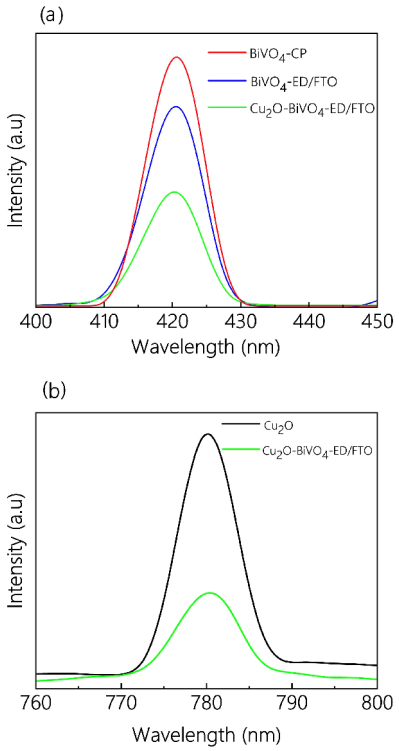


Fig. 4: PL spectra of $BiVO_4$-CP, $BiVO_4$-ED/FTO, $Cu_2O$-$BiVO_4$-ED/FTO at 210 nm excitation wavelength (a) and of $Cu_2O$, $Cu_2O$-$BiVO_4$-ED/FTO at 520 nm excitation wavelength (b)

### *Results of OER photoelectrochemical performance*

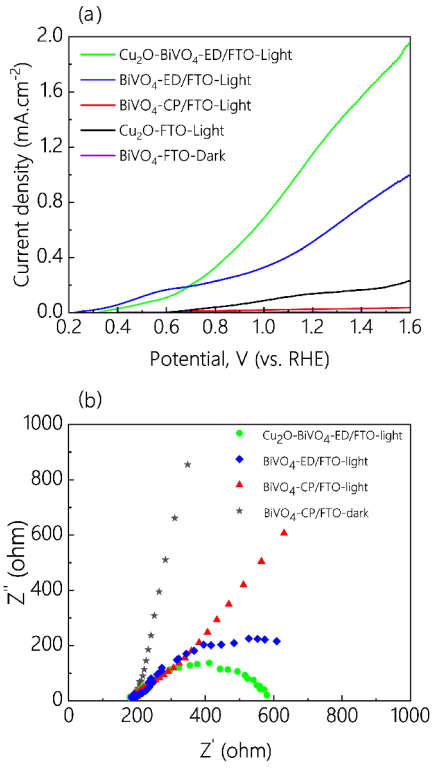


Fig. 5: Linear sweep voltammetry diagrams in the dark and under illumination (a) and Nyquist plot (b) of $BiVO_4$-CP, $BiVO_4$-ED/FTO, $Cu_2O$-$BiVO_4$-ED/FTO

https://doi.org/10.62239/jca.2025.007

To evaluate the photoelectrochemical catalytic ability of the materials for OER, LSV measurements were performed on the samples with results shown in Fig 5a. Obviously, in the absence of light, no current is observed on the FTO surface across the potential range of 0.2V to 1.6V versus RHE. However, under xenon lamp illumination, the photocurrent density on both $BiVO_4$ and $Cu_2O$ electrodes increases with rising potential. Comparing samples synthesized by precipitation, $BiVO_4$-CP/FTO, and electrodeposition methods, $BiVO_4$-ED/FTO, it is evident that the photocurrent density of electrochemically synthesized samples is far superior to that of samples synthesized through conventional chemical methods. At E=1.23V vs RHE, current density reaches 0.025 mA $cm^{-2}$ for $BiVO_4$-CP/FTO. and is 0.55 mA $cm^{-2}$ for $BiVO_4$-ED/FTO. The value of current density of $BiVO_4$-ED/FTO is comparable to that of $BiVO_4$ reported by Majumder et al. [12]. The enhancement in photocurrent density of $BiVO_4$-ED/FTO as compared to that of $BiVO_4$-CP/FTO is likely because the electrochemical synthesis method enables $BiVO_4$ to adhere strongly to the FTO surface, forming a uniform layer with smaller particle sizes and better interaction between the components in electrode. This facilitates easier movement of electrons and holes, enhancing their participation in electrode processes. The combination of $Cu_2O$ and $BiVO_4$ significantly enhances photocurrent density. While current density of $Cu_2O$/FTO and $BiVO_4$-ED/FTO samples are 0.142 mA $cm^{-2}$ and 0.55 mA $cm^{-2}$, respectively, the current density of $Cu_2O$-$BiVO_4$-ED/FTO reaches 1.23 mA $cm^{-2}$. These results suggest that heterojunction between $Cu_2O$ and $BiVO_4$ probably promotes separation of electrons and holes leading to better photocatalytic activity of the electrode material.

To evaluate the resistance to charge transfer at the interface between the electrode surface and the electrolyte during the OER, EIS measurements were conducted and the Nyquist plots were shown in Fig.5b. Typically, diameter of the semicircle in the high-frequency region reflects charge transfer resistance, $R_{ct}$. A smaller diameter indicates lower charge transfer resistance. Obviously, the semicircle diameter in the high-frequency region of $BiVO_4$-CP/FTO-dark is much larger than that of $BiVO_4$-CP-light, indicating the influence of illumination, which enhances the charge transfer at the interface between the electrode surface and the electrolyte. For the synthesized electrodes, the semicircle diameter decreases in the following order: $BiVO_4$-CP > $BiVO_4$-ED/FTO > $Cu_2O$-$BiVO_4$-ED/FTO. The charge transfer resistance of $BiVO_4$-CP, $BiVO_4$-ED/FTO and $Cu_2O$-$BiVO_4$-ED/FTO are determined to be 1728 Ω, 647 Ω and 401 Ω. The significantly lower value of charge transfer resistance for electrodeposited materials, $BiVO_4$-ED/FTO and $Cu_2O$-$BiVO_4$-ED/FTO as compared to $BiVO_4$-CP is likely attributed to the smaller particle size and the tighter adhesion of the deposited layer to the FTO surface, which may play a crucial role in the superior photoelectrochemical performance of the electrodeposited samples. Besides, the combined $Cu_2O$-$BiVO_4$-ED/FTO suggests the best efficient charge transfer and improved electron mobility at the interface between the electrolyte and the electrode with the lowest $R_{ct}$. Thus, the combination of $Cu_2O$ with $BiVO_4$ enhances the charge transfer ability of the materials. This improvement could be one of the factors contributing to the improvement of photoelectrocatalytic activity of the $Cu_2O$-$BiVO_4$-ED/FTO.

## Conclusion

In this study, $Cu_2O$ and $BiVO_4$ samples were successfully synthesized using different methods. The synthesis technique significantly influences crystallinity, morphology, particle size, ability of light absorption and photoelectrochemical performance of the electrode materials. $BiVO_4$ synthesized by electrochemical method ($BiVO_4$-ED) has lower crystallinity and significantly smaller particle sizes, therefore, exhibits higher photocurrent density (0.55 mA·$cm^{-2}$ at 1.23 V versus RHE) as compared to the materials synthesized by precipitation methods ($BiVO_4$-CP). When $Cu_2O$ and $BiVO_4$ are combined, the interaction between these two components in the material possibly reduces the recombination of electron-hole pairs, resulting in the higher charge transfer ability, $R_{ct}$=401 Ω, and better photocatalytic performance, with current density at 1,23 V vs RHE equal 1.23 mA $cm^{-2}$, showing its great potential for use as a photoanode material in photoelectrochemical water splitting.

## Acknowledgments

This research is funded by the Ministry of Education and Training under grant number B2022-SPH-15.

## References

1. T.W. Kim, K.S. Choi, Science 343 (6174) (2014) 990-994, https://www.science.org/doi/10.1126/science.1246913
2. B. Patial, A. Bansal, R. Gupta, S.K. Mittal, REVIC 44 (4) (2024) https://doi.org/10.1515/revic-2024-0009
3. R. M. Abdelfattah, M. Shaban, F. Mohamed, A.A.M. El-Reedy, H.M. Abd El-Salam, ACS Omeg, 6 (32) (2021) 20779–20789 https://doi.org/10.1021/acsomega.1c01802
4. A. Fujishima, K. Honda, Nature 238 (5358) (1972) 37-38 https://www.nature.com/articles/238037a0
5. N. Ma, C. Lu, Y. Liu, T. Han, W. Dong, D. Wu, X. Xu, Nano micro Small 20 (3) (2024) https://doi.org/10.1002/smll.202304839

6. H. T. Htet, Y. Jung, Y. Kim, S. Lee, ACS Appl. Mater. Interfaces 16 (39) (2024) 52383–52392 https://doi.org/10.1021/acsami.4c11095
7. G. Talasila, S. Sachdev, U. Srivastva, D. Saxena, S.S.V. Ramakumar, Energy Rep 6 (2020) 1963-1972 https://doi.org/10.1016/j.egyr.2020.07.024
8. C. Zhou, Z. S. Bellis, T. J. Smart, W. Zhang, L. Zhang, Y. Ping, M. Liu, Chem. Mate 32 (15) 2020) 6401–6409 https://doi.org/10.1021/acs.chemmater.0c01481
9. D. Jiang, L. Zhang, Q. Yue, T. Wang, Q. Huang, P. Du, Int. J. Hydrogen Energy 46 (29) (2021) 15517-15525 https://doi.org/10.1016/j.ijhydene.2021.02.094
10. H. Wu, S. Qu, Z. Xie, Y. H. Ng, ACS Appl. Energy Mater. 5 (7) (2022) 8419–8427 https://doi.org/10.1021/acsaem.2c00963
11. S. Majumder, X. Su, K. H. Kim, Surfaces and Interfaces 39 (23) (2023) 102936 https://doi.org/10.1016/j.surfin.2023.102936
12. G. Liu, Y. Zhu, H. Gao, S. Xu, Z. Wen, L. Sun, F. Li, ACS Catal. 13 (13) (2023) 8445–8454 https://doi.org/10.1021/acscatal.3c01235
13. M. Zhou, Z. Guo, Z. Liu, Appl. Catal., 260 (2020) 118213 https://doi.org/10.1016/j.apcatb.2019.118213
14. J. Heo, H. Bae, P. Mane, V.Burungale, C. Seong, J. S. Ha, ACS Omega 8 (36) (2023) 32794–32803 https://doi.org/10.1021/acsomega.3c03585